Journal of Indian Geomorphology
Volume 13, 2025 ● ISSN 2320-0731
Indian Institute of Geomorphologists (IGI)

An Assessment of Cyclonic Vulnerability of West Bengal Coast

Ratna Khoso[1] and Sukla Hazra[1]
[1]*East Calcutta Girls' College, Kolkata, West Bengal - 700089*
E-mail: ratna.khoso2013@gmail.com (Corresponding author)

Abstract: *The Bay of Bengal frequently experiences tropical cyclones, leading to a vulnerable situation in the coastal region. The main aim of this study is to conduct a cyclonic vulnerability assessment through selected cyclonic storms that occurred from 2001 to 2024 in forty-four blocks along the West Bengal coast. To assess the vulnerability of this area, major indicators have been selected that represent physical and natural characteristics, cyclonic hazard exposure, land use and land cover, and socio-economic status. Twenty-four indicators have been categorised into three components—exposure, sensitivity, and adaptive capacity—recommended by the Intergovernmental Panel on Climate Change (IPCC) for the vulnerability assessment. The Principal Components Analysis method has been used to assign weight to develop the composite indicators for the cyclonic vulnerability index. Keiser-Meyer-Olkin and Bartlett's tests have been implemented to check sampling adequacy, which is 0.71. Results indicate that East Medinipur is less exposed and sensitive to cyclonic hazards compared to the Indian Sundarbans region. This is due to the greater impact of storm surges through the deltaic estuaries of the Sundarbans. Additionally, the open coastal environment of East Medinipur influences the conditions of the coastal blocks, which are more enclosed to the sea. Adaptive capacity is comparatively very high in Sagar, Namkhana, Mathurapur II, and Gosaba. Seven blocks are highly cyclonically vulnerable (0.26-0.63), and three blocks are very highly cyclonically vulnerable (> 0.64) in the Indian Sundarbans region due to low elevation, low social awareness, and insufficient infrastructural facilities.*

Keywords: Exposure, Sensitivity, Adaptive capacity, Inundation, Vulnerability

Introduction

The Intergovernmental Panel on Climate Change (IPCC) report 2007 identified coastal areas as hot spots for climate change and extreme weather events, including cyclones (IPCC, 2007; EEA, 2006). Warm tropical oceans often denote low air pressure, high wind speeds, and heavy rainfall, which are the ideal conditions for forming a tropical cyclone (Wong *et al.,* 2008). The extent of damage caused by these weather events to coastal areas and their interiors depends on the cyclone's intensity (De *et al.,* 2020). The local damages can also be indicated by the cyclonic intensity after landfall on the landmass (Hoque *et al.*, 2016). Between

1980 and 2019, the Arabian Sea and the Bay of Bengal (BoB) witnessed an average occurrence of 1.58 and 3.25 tropical cyclones per year, respectively (Duan *et al.*, 2021). Over the last two decades, the BoB has been considered a cyclone-prone coastal area (Mondal *et al.*, 2022). Andhra Pradesh, Odisha, and West Bengal (WB) states are particularly vulnerable to these extreme weather events, resulting in severe socio-economic losses (Chittibabu *et al.*, 2004). Moreover, these coastal states are also vulnerable to other climatic factors, such as sea-level rise (Siegel, 2020), storm surges (Chen *et al.*, 2020), and flooding (Gupta, 2020). During a cyclonic period, there is a sudden increase in the vulnerability of coastal communities.

Vulnerability is a complex phenomenon that involves various factors. The vulnerability index typically comprises sub-components that aggregate the contributing variables (Below *et al.*, 2012). Coastal hazard vulnerability arises from environmental, economic, and social factors (Ummenfer *et al.*, 2017). Coastal areas are naturally productive and densely populated regions (McGranahan *et al.*, 2007), so hazards affect natural and human systems, including forests, rivers, ponds, lakes, and socio-economic elements such as agriculture, settlement, transport, health, livelihood, and communities. In this context, vulnerability is expressed in several quantitative indices, which is a crucial step towards risk assessment and management (Romieu *et al.*, 2010). These effects highlight the need for interventions in different spatio-temporal scales related to socio-economic and environmental systems. This event makes social infrastructure vulnerable, emphasising that it requires preparation, coping, and recovery from the impacts of its vulnerability (Rubinato *et al.*, 2020).

The distribution of tropical cyclones (TCs) varies across the states, with Odisha, Andhra Pradesh, WB, and Tamil Nadu witnessing the highest frequency of storm occurrences. According to the Indian Meteorological Department (IMD), nearly 534 cyclonic storms occurred in the BoB from 1891 to 2023. From 1950 to 1980, the frequency of cyclones was higher, but it decreased in subsequent years. However, since 2005, the frequency of cyclones has increased again. 60 cyclonic storms have occurred with different intensities along the eastern coast of India between 2001 to 2023. Out of 60, nine TC affected the WB coast (Table 1), which are distinct in their characteristics (intensity, storm surge, inundation amount, tidal status, and duration). This is an important part of this research that has considered all types of cyclones from cyclonic storm (CS) 'Rashmi' (2008) to super cyclonic storm (SCS) 'Amphan' (2020). Thus, assessment reflects the present adaptive capacity (AC) with different levels of hazardous situations, exposure, and sensitivity in different cyclones.

The studies conducted on coastal Bangladesh have primarily focused on various aspects such as hazard warning and evacuation systems (Shoji and Murata, 2021). Some researchers published vulnerability assessments of the Bangladesh coast, which were based on some common indicators (Hoque *et al.*, 2021), while Hinkel (2011) and Mondal *et al.* (2021) conducted their studies with standardization, assigning weighting, and aggregation methods. Behera *et al.* (2022) studied the assessment of tropical cyclone 'Amphan' along the eastern Indian coast and detected the inundated area. Sharma *et al.* (2020) used real-time satellite data to delineate and monitor flood-affected areas

during the SCS 'Amphan' in WB. Similarly, few scientists have assessed the effect of TCs Aila (2009), Bulbul (2019), Amphan (2020), and Yaas (2021) (Kar and Bandyopadhyay, 2015; Hassan *et al.*, 2020; Das *et al.,* 2020; Mishra *et al.,* 2021; Halder *et al.*, 2021; Paul and Chowdhury, 2021). Based on the above reviews, most studies rely on common vulnerability indices without incorporating advanced geospatial techniques or real-time satellite data to enhance accuracy in inundation mapping. The absence of block-level vulnerability assessments limits the applicability of findings for localised disaster management and policy interventions. This study addresses these gaps by developing a Cyclone Vulnerability Index (CVI) that integrates exposure, sensitivity, and adaptive capacity, providing a more holistic framework for assessing cyclonic hazards in coastal West Bengal.

Objectives

The objectives of this study are —(i) to determine the hazardous exposure and sensitivity to cyclonic events in the Sundarbans and East Medinipur (EM) blocks. (ii) to measure the AC of selected coastal blocks due to the cyclones and (iii) to establish an appropriate Cyclone Vulnerability Index (CVI) for the coastal area. We have combined the IPCC Vulnerability Framework (Lavell *et al.*, 2012) and also the Coastal Specificities Framework (Bjarnadottir *et al.*, 2011; Wu, 2021), where indicators of Exposure, sensitivity, and AC were considered three dimensions of cyclonic vulnerability based on the character of study area and facing cyclones (Krishnamurthy *et al.*, 2011). This approach enables us to obtain both aggregated and individual rankings of various factors and vulnerability dimensions within a spatial

Table 1: Details of selected tropical cyclones along the Odisha, West Bengal and Bangladesh coasts from 2001 to 2024. Data sources: IMD report (https://rsmcnewdelhi.imd.gov.in) and NASA/POWER CERES/MERRA2 Native Resolution Daily Data (https://power.larc.nasa.gov/data-access-viewer/).

Cyclone Intensity	Cyclone	Year	Landfall day and month	Place of landfall	Wind speed (km h^{-1})	Wind pressure (mb)	Tidal condition
Cyclonic Storm (CS)	Rashmi	2008	26th Oct	Bangladesh coast	38–62	984	Low tide
	Sitrang	2022	24th Oct	Bangladesh coast	52–69	994	High tide
Severe Cyclonic Storm (SCS)	Sidr	2007	15th Nov	Bangladesh coast	55–78	918	Low tide
	Aila	2009	25th May	Sagar Island	61–80	967	High tide
	Remal	2024	26th May	Khepupara, Bangladesh	45–61	978	Low tide
Very Severe Cyclonic Storm (VSCS)	Bulbul	2019	9th Nov	Sundarbans, Bangladesh	50–69	976	Low tide
	Yaas	2021	25th May	Balasore, Odisha	45–84	970	High tide
Extremely Severe Cyclonic Storm (ESCS)	Fani	2019	3rd May	Puri, Odisha coast	53–73	932	Low tide
Super Cyclonic Storm (SCS)	Amphan	2020	20th May	Sundarbans, India	70–95	925	Low tide

context. Appropriate adaptation and coping strategies for coastal communities are to be marked (Smit and Wandel, 2006) in cyclone hazard-prone vulnerable regions. Thus, the authors applied the CVI framework to assess the vulnerable situation associated with cyclonic hazards. This study is critical for disaster preparedness and climate adaptation. Quantifying vulnerability and providing a structured assessment model enables data-driven decision-making for coastal resilience planning. The findings can be scaled and adapted for other cyclone-prone regions globally, making it a valuable contribution to climate risk research.

Study area

The eastern coast of the Indian subcontinent boasts of unique floral and faunal biodiversity, diverse geomorphic features, and anthropogenic intrusions (Bhakat, 2001). For our study, we have selected the community development (CD) blocks of EM and the Indian Sundarbans region (ISR) under the North and South 24 Parganas districts, which covers 157.5 km coastal stretch of WB (Fig. 1). The study area lies between 22°31′ N to 21°38′ N and 87°27′ E to 89°05′ E (Fig. 1). The primary physical features of EM comprise of estuaries, tidal flats, sandy beaches, spits, bars, salt marshes, and dunes (Das and Dandapath, 2014). On the other hand, the ISR mainly consists of tidal estuaries, clay-silt composed islands, and dense mangrove forests (Bandyopadhyay, 2007).

A cyclone cannot be confined by administrative units. However, demographic data is required to measure the effects of cyclones, adaptability, mitigation, or capability of people and plan for protection of the people from extreme weather in the future. The present research has taken population data at the block level to measure cyclonic vulnerability. The study area covers forty-four administrative blocks for the above-mentioned requirement.

Database and methodology

Data source

The study is based on satellite data that is freely accessible. Permanent water bodies and inundation areas have been identified by processing the Synthetic Aperture Radar (SAR) based high-resolution (5 m) level 1 Ground Range Detected (GRD). All Sentinel 1 images have been downloaded from the Alaska homepage (https://asf.alaska.edu/). SAR is a remote sensing method that collects data regardless of light or weather conditions. Sentinel 2 images on 14th January 2024 have been used to prepare a Land use and land cover (LULC) map to extract the present area of forest, inland water bodies, built-up area, and cultivated land (https://scihub.copernicus.eu/). This LULC map has been verified by some ground truth GPS locations of Minakhan, Haroa, Hingalganj, Hasnabad, and Sandeshkhali I and II. The LULC classes are also verified by Google Earth Pro. The accuracy test is crucial in generating a reliable supervised classification (Joy *et al.*, 2019). This research has utilised the Kappa Statistical Coefficient method, recognised as one of the most reliable approaches (Kanga and Singh, 2017). The study followed a similar procedure for the Kappa test as previous studies (Kanga *et al.*, 2020). The detailed description of the twenty-four indicators and the relevant formulas used are included in Table 2 and Table 3 respectively.

$$K = \frac{\left\{N\Sigma_{i=1}^{r}(X_{ii}) - N\Sigma_{i=1}^{r}(X_{i+} + X_{+i})\right\}}{N^2 - \Sigma_{i=1}^{r}(X_{i+} + X_{+i})} \quad \text{...(Eq. 1)}$$

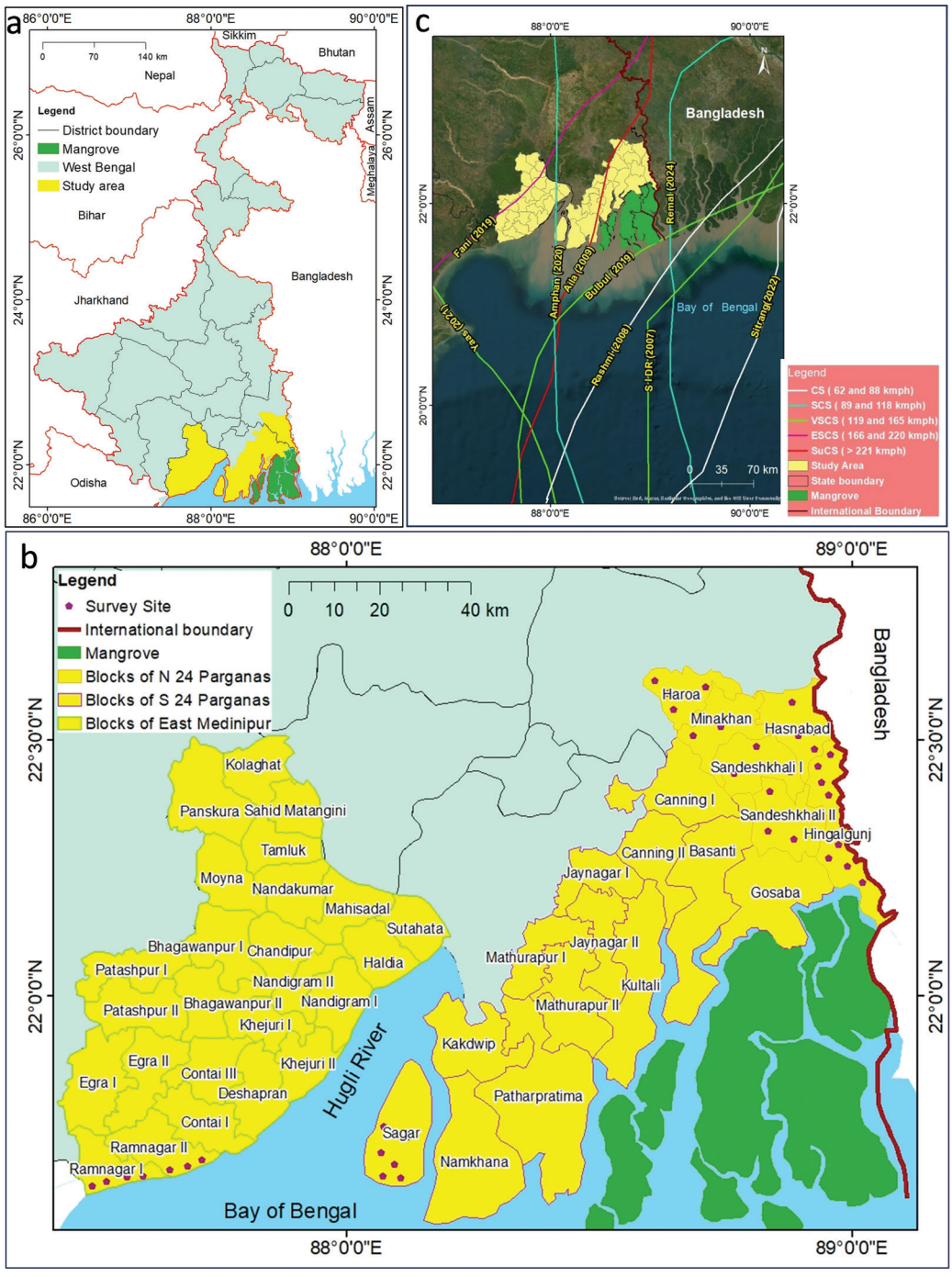

Figure 1. (a) The location of the study area within West Bengal, (b) Location of CD blocks in East Medinipur and Sundarbans, highlighting surveyed locations selected to validate the land use and land cover classification map, (c) Track lines of selected tropical cyclones sourced from the IMD official site.

Where r represents the number of rows in the error matrix; X_{ii} is the number of observations in row i and column i; X_{i+} represents the total of observations in row i; X_{+i} expresses the total of observations in column i, and N represents the total number of observations included in the matrix. The accuracy assessment results showing an overall accuracy found from the random sampling process is nearly 92%.

Table 2. Components and indicators of cyclonic vulnerability index and their details.

Components	Indicators	Data source	Effect direction
Exposure	Area of flood inundation in km^2 (E1)	Sentinel 1 SAR-C images	+ ve
	Wind speed in km hr^{-1} (E2)	NASA/ POWER CERES/ MERRA2 Native Resolution Daily Data	+ ve
	Storm surge in m (E3)	Indian National Centre for Ocean Information Services	+ ve
	Flood duration in day (E4)	Sentinel 1 SAR-C images	+ ve
	Forest area in ha (E5)	LULC map of Sentinel 2 images on 14th January, 2024	− ve
	Proximity to the drainage in m (E6)	Open series map from SOI, Scale of 1:50000 (F45K6, F45K7, F45K8, F45K10, F45K11, F45K12, F45K14, F45K15 and F45K16)	+ ve
	Elevation in m (E7)	SRTM DEM, USGS earth explorer	+ ve
	Inland water bodies in ha (E8)	LULC map of Sentinel 2 images on 14th January, 2024	− ve
	Distance from coastline in km (E9)	Google Earth Pro	− ve
Sensitivity	Built-up area per ha (S1)	LULC map of Sentinel 2 images on 14th January, 2024	+ ve
	Cultivated land in ha (S2)	LULC map of Sentinel 2 images on 14th January, 2024	+ ve
	Kuccha house in % (S3)	Socio Economic and Caste Census (2011)	+ ve
	Poverty ratio in % (S4)	District Human Development Report of 2009	+ ve
	Dependency ratio in % (S5)	District Census Handbook of 2011	+ ve
	Bore well/Tube well in % (S6)	District Census Handbook of 2011	− ve
	Marginal workers in % (S7)	District Census Handbook of 2011	+ ve
	Number of livestock and poultry in % (S8)	District Census Handbook of 2011	+ ve

Components	Indicators	Data source	Effect direction
Adaptive capacity	Literacy rate in % (AC1)	District Census Handbook of 2011	− ve
	Medical amenity in % (AC2)	District Census Handbook of 2011	− ve
	Shelter accessibility in m (AC3)	Environment and Social Screening Report, West Bengal	− ve
	Workforce participation rate in % (AC4)	District Census Handbook of 2011	− ve
	Approach by pucca road in % (AC5)	District Census Handbook of 2011	− ve
	Villages having power supply in % (AC6)	District Census Handbook of 2011	− ve
	Transport communications in % (AC7)	District Census Handbook of 2011	− ve

Block-level administrative data have been obtained from the District Census Handbook of EM, North 24 Parganas, and South 24 Parganas for the year 2011 to prepare the CVI of the study area. Other important reports of cyclonic conditions have been acquired from the IMD (https://mausam.imd.gov.in) and the Regional Specialised Meteorological Centre (RSMC) (https://rsmcnewdelhi.imd.gov.in), specifically cyclone track, sea condition, wind speed, landfall time, and cyclone formation (Table 1). Other climatic data like wind speed has been collected from NASA/POWER CERES/MERRA2 Native Resolution Daily Data (https://power.larc.nasa.gov/data-access-viewer/).

Table 3. Application of standardised formulas for selected indicators.

Components	Indicators	Formula
Sensitivity	Dependency ratio (%)	100 x (Population (0−14) + Population (65+)) / Population (15−64)
Adaptive capacity	Literacy rate (%)	(Number of literate persons)/ (Total population) x 100
	Workforce participation rate (%)	(Number Employed/Total number of working age population) x 100

Indicator selection

The indicators used in this study are based on the elements of physical, natural, land use and land cover, social and demographic, economic systems, and coastal hazard exposure (Table 2). A total of 24 indicators has been calculated at the census tract scale (256 tracts) and municipality scale (24 municipalities). Although the indicators selected in this study cannot be considered an exhaustive description of different tracts and municipalities' physical and social contexts, they do provide a broad qualification of physical traits and socio-economic situation observed in the coastal indicators depending upon the type of problems, the nature of the data, and the objectives of analysis (Kotzee and Reyers, 2016).

Composite indicators and data normalisation

The Vulnerability Index is an appropriate method for the present research. It follows the composite framework method of three main dimensions: exposure, sensitivity, and AC which is recommended by the IPCC (Patwardhan *et al.*, 2007). A composite indicator combines individual indicators representing different dimensions of a hypothesis to analyse it. The work has been done in six steps: variable selection, data normalization, multivariate statistical analysis, weight derivation, indicators composition, and descriptive statistics of the obtained composite indicators. So, the selected twenty-four variables are approved as very significant for the present research. To establish a relationship between the selected indicators, absolute values were standardised. However, since the indicators were measured on different scales, we used the Z-score normalisation method Eq. (2) and (3). This method distributes the values uniformly on a scale with mean values of 0 and standard deviations of 1, making it essential for standardization (Xia *et al.*, 2021). The following expression was applied:

$$Z = \frac{x - \mu}{\sigma}$$ when x is positive indicator ... (Eq. 2)

$$Z = \frac{\mu - x}{\sigma}$$ when x is negative indicator ... (Eq. 3)

Here, Z represents the standardised indicator, x represents the original input indicator, μ is the arithmetic mean of x, and σ represents the standard deviation of x. This calculation was carried out using IBM SPSS Statistics 25 software.

Principal Component Analysis (PCA) for dimension reduction

The PCA method is utilised in this study to determine whether the selected sub-components are suitable for the current research. Cutter *et al.* (2003) used this method to evaluate the socio-economic vulnerability of some states of US by assessing the hazard impact. Similarly, Kleinosky *et al.* (2007) applied PCA to assess vulnerability in Virginia due to storm surge and sea level rise. Hufscmidt (2008) also employed PCA in his landslide research to measure vulnerability and resilience in the Western Hutt Hills, New Zealand. This study computed twenty-four indicators by using Kaiser-Meyer-Olkin (KMO) and Bartlett's test to measure sampling adequacy and sphericity checks (Bartlett, 1950) in SPSS. The KMO index varies from 0 to 1 and summarises the sampling adequacy in the 0.90s (excellent), 0.80s (good), 0.70s (fair), 0.60s (poor), 0.50s (unacceptable), and below 0.50 (unacceptable) for conducting factor or component analysis (Kaiser and Rice, 1974). The sampling adequacy of this study is classified under the fair category with a value of 0.71, and the 'P' value is 0, which is less than the critical value of 0.05, thus annulling the null hypothesis and indicating that the data is appropriate for PCA. Out of the twenty-four selected indicators, seven components have eigenvalues greater than 1. The PCA of the seven components explains 74.28% of the variability in the data (Table 4).

Table 4. Total explained variance

Component	Initial eigenvalues			Extraction sums of squared loadings			Rotation sums of squared loadings		
	Total	% of Variance	Cumulative %	Total	% of Variance	Cumulative %	Total	% of Variance	Cumulative %
1	7.28	30.32	30.32	7.28	30.32	30.32	4.38	18.27	18.27
2	3.65	15.22	45.54	3.65	15.22	45.54	3.43	14.30	32.57
3	2.43	10.13	55.67	2.43	10.13	55.67	3.35	13.94	46.50
4	1.86	07.75	63.42	1.86	07.75	63.42	3.15	13.11	59.62
5	1.50	06.24	69.66	1.50	06.24	69.66	2.18	9.10	68.71
6	1.11	04.62	74.28	1.11	04.62	74.28	1.34	5.56	74.28

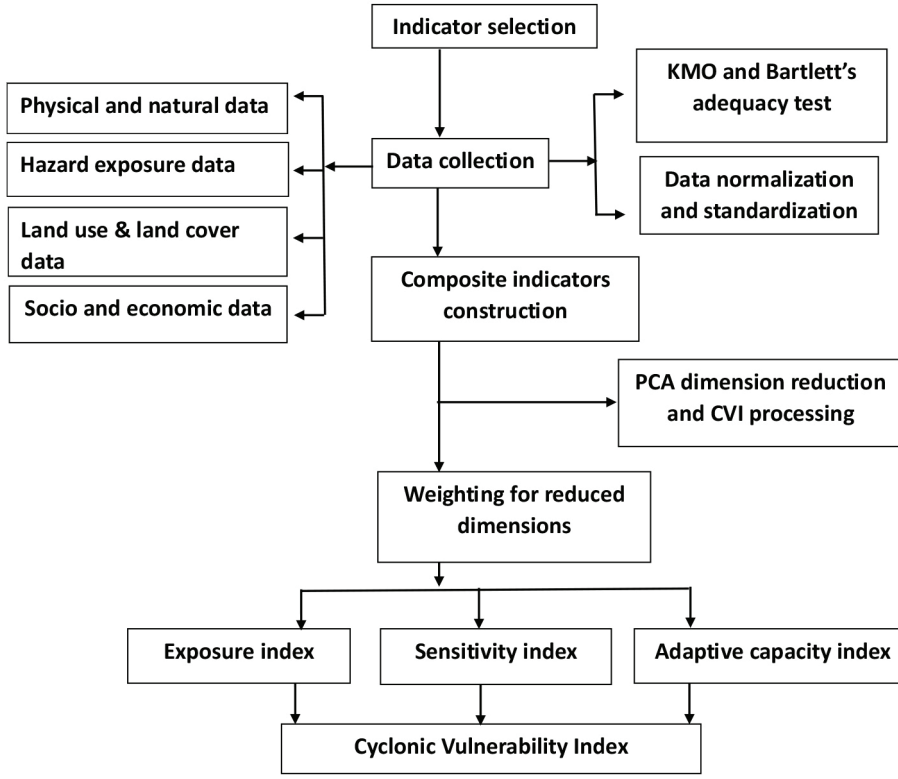

Figure 2. Method of assessing Cyclonic Vulnerability Index (CVI), adapted from Wu (2021) with modifications by the authors.

Weighting approach and Cyclonic Vulnerability Index (CVI)

Several critical steps were followed to calculate the CVI of the selected CD Blocks, expressed through statistical equations (Fig. 2). The principal components were obtained after performing PCA, and the weight of each indicator was extracted based on the factor loading from the rotated components matrix and the cumulative eigenvalues of the rotation sums of squared loadings. Table 5 shows the steps and their explanations.

Results

Principal Component Analysis

The results of the PCA computation showed the composition of a matrix containing data on 24 indicators of 44 blocks of EM and ISR along the WB coast. These results are presented in Table 6. Six principal components (PCs) were extracted, with eigenvalues greater than 1 (Fig. 3), indicating that they covered 74.28% of the variance of the data and included a large number of input variables. The first six PCs are extraction

Table 5. Equations for weighting approach.

Steps for PCA	Formula	Explanation	Equation number
IVI_{ji}	$\sum_{k=1}^{K=n} W_{kj} I_{ki}$	IVI_{ji} = the intermediate vulnerability indicator for the component j and the tract i, Wk_j =the weight of indicator k in the component j, Iki = the normalised indicator k achieved by the tract i,	4
Wkj	$\frac{factor\ loading_{kj}^2}{eigenvalue_j}$	K_j = the value of the factor loading of indicator k in the principal component j, $eigenvalue_j$ = the eigenvalue of the jth principal component	5
CVI_i	$\sum_{k=1}^{K=n} a_j IVI_{ji}$	CVIi (Cyclonic Vulnerability Index) = the value of the composite indicator for tract i, αj = the weight applied to the intermediate vulnerability indicator j.	6
EI_i	$\sum_{k=1}^{K=n} a_j IVI_{ji}$	EI_i (Exposure Index) = the value of the exposure indicators for tract i, αj = the weight applied to the intermediate vulnerability indicator j.	7
SI_i	$\sum_{k=1}^{K=n} a_j IVI_{ji}$	SI_i (Sensitivity Index) = the value of the sensitivity indicators for tract i, αj = the weight applied to the intermediate vulnerability indicator j.	8
ACI_i	$\sum_{k=1}^{K=n} a_j IVI_{ji}$	ACI_i (Adaptive Capacity Index) = the value of the adaptive capacity indicators for tract i, αj = the weight applied to the intermediate vulnerability indicator j.	9
Aj	$\frac{eigenvalue_j}{\Sigma_{j=1}^{j=5} eigenvalue_j}$	Eigenvaluej = the eigenvalue of the jth principal component	10

sums of squared loadings, which are 30.32%, 15.22%, 10.13%, 7.75%, 6.24%, and 4.62% respectively (Table 4). The communality values, which represent the squared multiple correlation of six PCs for each indicator, reflect the contribution of the indicators. High communality values indicate more explained variance in the correlation matrix, while low values indicate more unexplained variance (Table 6). The communality values of some indicators, such as the NLP, BW/TW, FA, IWB, AFI, WPR, LR, and DR are less than .70, indicating a low influence on the CVI. The communality values of other indicators such as PL, BUA, CA, SS, MA, ELV, APR, and MW are between .70 to .80, indicating a significant impact on the CVI. The communality values of some indicators such as DC, FD, VHPS, PD, SHA, WS, and KH are greater than .80, indicating the most significant influence on the CVI. There are six categories based on PCs. Four indicators are included in PC 1, namely FD, DC, ELV, and IWB. Four indicators are comprised in PC 2, namely MA, TCM, APR, and BW/TW. Four indicators are contained in PC 3, namely FA, BUA, PR, and LR. Three indicators are included in PC 4, namely WS, SS, and WPR. Two indicators are contained in PC 5, namely MW and KH (Table 6).

Table 6. Rotated Component Matrixa , where a indicates rotation converged in 17 iterations. Extraction Method: Principal Component Analysis, Rotation Method: Varimax with Kaiser Normalisation.

Indicators	Component						Communalities
	1	2	3	4	5	6	
Flood duration (FD)	0.888	0.104	0.275	−0.099	−0.061	−0.094	0.897
Distance from coastline (DC)	0.827	−0.008	0.127	−0.456	−0.143	−0.078	0.935
Elevation (ELV)	−0.814	−0.178	−0.050	−0.205	−0.113	0.106	0.763
Inland water bodies (IWB)	0.708	0.258	−0.055	−0.289	0.130	0.039	0.673
Poverty level (PL)	0.565	0.344	0.491	0.256	−0.067	0.050	0.751
Percent of villages having power supply (VHPS)	−0.555	−0.105	−0.437	−0.482	−0.033	0.296	0.832
Medical amenity (MA)	−0.051	0.823	0.052	−0.076	0.156	−0.140	0.732
Transport communications (TCM)	0.364	0.745	−0.105	−0.013	0.095	−0.067	0.713
Approach by pucca road (APR)	0.429	0.693	0.087	0.337	0.061	0.106	0.799
Bore well/ tube well (BW/TW)	−0.122	−0.602	−0.074	−0.023	0.252	0.500	0.697
Forest area (FA)	0.070	−0.026	0.720	−0.065	0.061	0.114	0.544
Built−up area (BUA)	0.024	−0.093	0.652	0.200	0.552	0.113	0.792

Indicators	Component						Communalities
	1	2	3	4	5	6	
Proximity to drainage (PD)	0.260	0.558	0.610	0.120	0.285	0.140	0.867
Literacy rate (LR)	−0.235	−0.033	−0.607	0.384	0.095	0.286	0.662
Cultivated land (CL)	0.000	0.533	0.575	0.209	0.143	0.181	0.712
Shelter accessibility (SHA)	0.438	0.457	0.502	0.462	0.128	0.105	0.895
Wind speed (WS)	−0.359	0.060	0.338	0.750	0.093	−0.037	0.820
Storm surge (SS)	0.201	0.410	0.083	0.742	−0.101	0.019	0.776
Workforce participation rate (WPR)	−0.167	−0.073	−0.200	0.736	0.219	0.095	0.672
Dependency rate (DR)	0.010	−0.290	−0.169	0.423	−0.349	−0.237	0.470
Marginal workers (MW)	−0.032	0.128	0.020	−0.020	0.848	0.049	0.740
Kuccha house (KH)	0.141	0.128	0.331	0.289	0.721	−0.317	0.850
Area of flood inundation (AFI)	0.308	0.093	−0.191	−0.063	0.289	−0.589	0.574
Number of livestock and poultry (NLP)	0.390	−0.007	0.432	−0.014	0.275	0.495	0.660

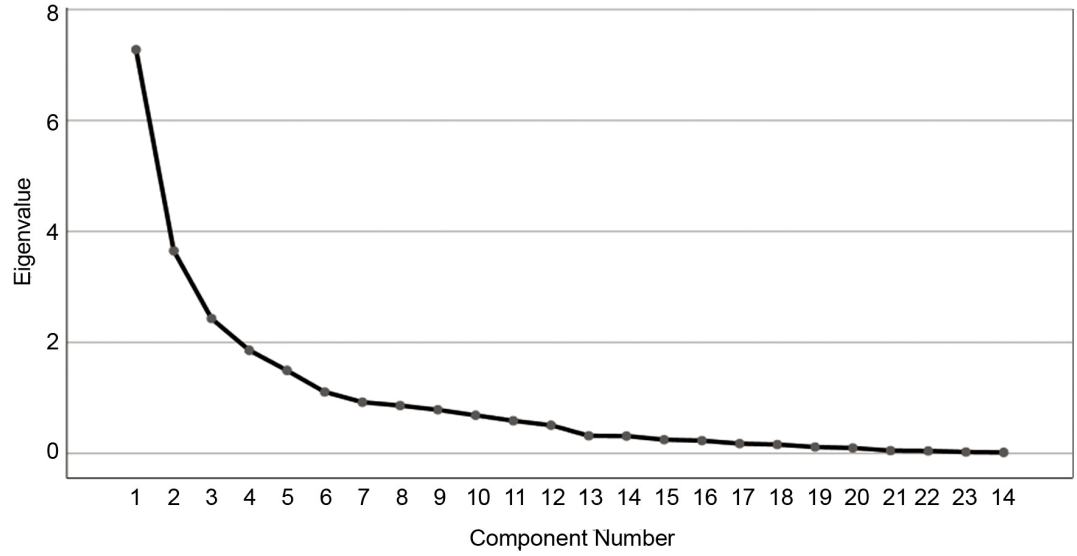

Figure 3. Scree plot showing distribution of components exceeding an eigenvalue of 1, indicating significant factor retention.

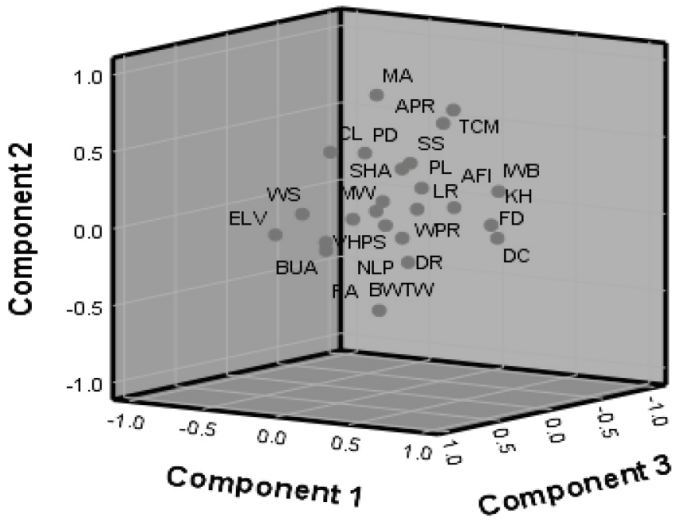

Figure 4. Visual representation of component loadings in rotated space, highlighting factor clustering and structural relationships.

Correlation among the selected indicators

Table 7 displays the Pearson correlations among selected indicators based on the correlation coefficient matrix. The absolute values of the correlation coefficients below 0.30 indicate poor linear relationships. The table shows moderate (absolute value ranging from 0.30 to 0.50) and strong (>0.50) correlations with their positive and negative classifications (Wu, 2021). The preliminary screening of the indicators reflects the intuitive relationships and grouping features among them. The ELV has a strong negative correlation with FD, and the FD shows a strong positive correlation with DC. As PD increases, CL and BUA also increase because people avoid the saline water of tidal creeks for cultivation and build their houses at a distance from those creeks. Nowadays access to pucca roads, together with adequate and proper shelter also increases significantly with proximity to drainage due to changes in the transport system and enhancement of AC. SS increases with WS. After landfall, the intensity of the cyclone decreases as it moves towards inland from the coastline. MA is highly available where APR and TCM are high. SA is available with the APR. However, the PR increases with an increase in FA, indicating that poor people have built their homes near the forest. Low-elevated lands are highly correlated with the number of inland water bodies. The high SS has highly affected the WPR, as per Table 7, and this is notable for socio-economic losses. These indicators exhibit a clustered feature; natural indicators correlate with hazard exposure, while socio-economic indicators show high internal correlations with hazard exposure as well (Fig. 4). The details of the correlation among indicators are furnished in Table 7. The correlation structure in Table 7 indicates that a data reduction will be rational (Riitters *et al.,* 1995). Therefore, the PCA method is appropriate for the current study.

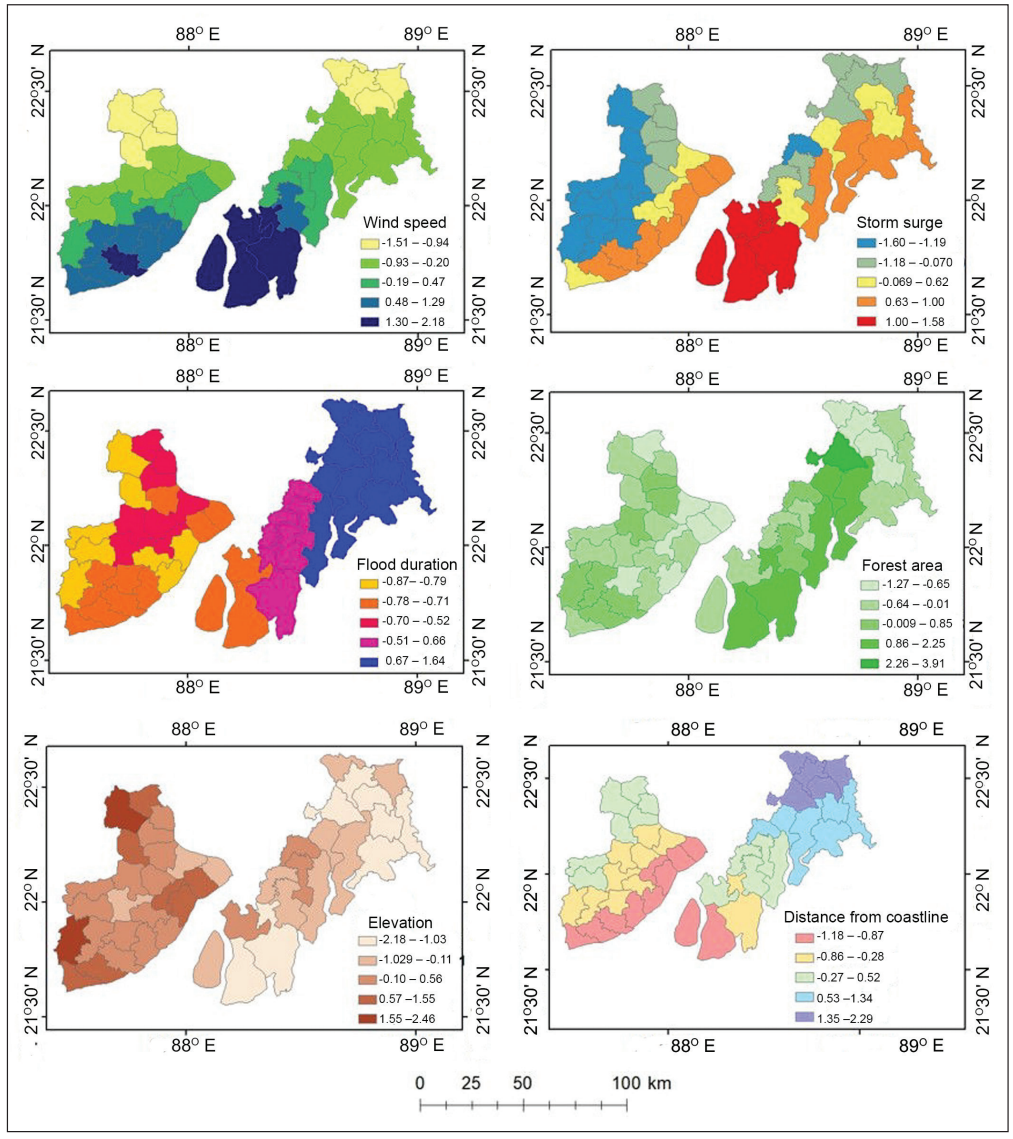

Figure 5. Spatial distribution of exposure Index indicators mapped using standardised values to highlight regional variations and risk intensity.

Exposure Index (EI) along the West Bengal coast

The EI is calculated on the physical condition of the affected area and is divided into five classes based on Jenks natural breaks. The Patharpratima, Kultali, Basanti, Gosaba, Sandeshkhali II, and Canning II CD blocks of ISR record a very high EI from 0.21 to 0.56. The nine CD Blocks of ISR include a high EI with the value from 0.04 to 0.20. The EI shows that the combination of low-lying elevation, high inundation, high SS height, high proximity to drainage, and distance from the coastline form most of the blocks situated

adjacent to the coastal areas which are highly exposed to cyclonic events (Fig. 5). The southern blocks of Sundarbans are covered and protected by mangroves that can prevent the cyclonic effect. High ELV is negatively correlated with cyclonic SSs. Tidal rivers along the coast are the main way of seawater intrusion into the coastal blocks, with several creeks and small channels. Thematic maps of exposure indicators such as proximity to drainage and SS height show high values near the coast (Fig. 5). In Figure 6, eleven C.D. Blocks have moderate EI of −0.10 to 0.03 because of moderate and greater proximity to drainage, moderate forest cover, and distance from the coastline. These eleven CD Blocks are Contai I, Ramnagar I and II, Deshopran, Nandigram I, Moyna, Tamluk, Mathurapur I, Jaynagar I, Jaynagar II, Minakhan. Low Exposed C.D. Blocks are Egra I, Khejuri I and II, Nandigram II, Chandipur, Mahishadal, Nandakumar, Haldi, Sahid Matangini, Mahishadal, Panskura with the value −0.21 to −0.09. There are seven potentially exposed C.D. Blocks included with the values −0.31 to −0.22 because of less open-sea effect and less affected indicators.

Sensitivity Index (SI) along the West Bengal coast

The blocks connected to the mainland were highly sensitive due to the high density of buildings, a large area of cultivation, and the presence of KH. The lowlands in ISR and EM, near the coast, were particularly risky and sensitive to cyclones due to salinity and waterlogging. Most blocks showed high sensitivity due to a high DR and poverty ratio in the southern CD Blocks of ISR. The socio-economic highly sensitive zone contains high concentration of marginal workers and the ISR was maximum when compared to EM

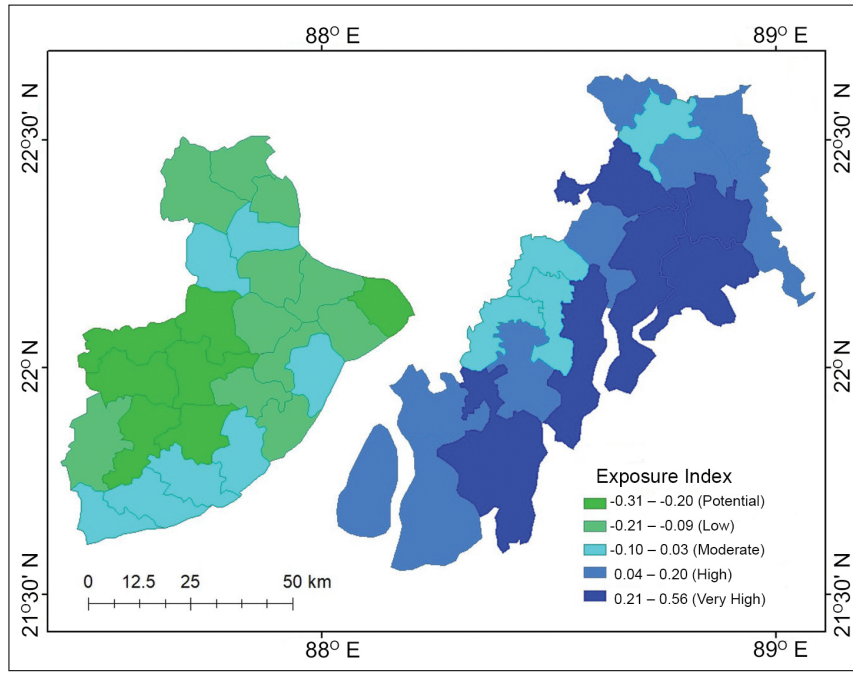

Figure 6. Spatial variation in Exposure Index (EI) at the block level within the study area, highlighting standardised risk distribution and regional disparities.

(Fig. 7). The combination of eight socio-economic indicators of the coastal blocks of WB expressed the result of the sensitivity index, which is classified into 5 classes based on Jenks's natural breaks. In Patharpratima, Basanti, and Gosaba CD blocks of ISR show high intensity of agriculture and built-up area. So, the extreme weather in these zones spoiled crop production and damaged properties that recorded a very high SI ranging from 0.28 to 0.69. The Sagar, Namkhana, Kultali, Contai II, and Hingalganj CD blocks of ISR and East Medinipur included a high sensitivity index ranging from 0.08 to 0.27 due to damage of agriculture and kutcha houses. Nine CD Blocks of EM and seven CD Blocks of Sundarbans were moderately sensitive with a value of −0.07 to 0.07. Sixteen C.D. Blocks of the study area were low and potentially sensitive (Fig 8). Infrastructure facilities and good transport may help to reduce the sensitivity to cyclones.

Adaptive Capacity Index (ACI) along the West Bengal coast

The ACI is the result of an amalgamation of seven AC indicators of the coastal blocks of WB (Fig. 9). The ACI is divided into five classes based on Jenk's natural breaks. In the study area, twenty-five of the forty-four CD Blocks are classified as having low to moderate adaptive capacity. These CD Blocks are generally lacking in infrastructure development. The highest ACI is recorded from 0.24 to 0.45 in Sagar, Namkhana, Mathurapur II, and Gosaba of ISR. The blocks with a high ACI have an index value of 0.07 to 0.23 and include Patharpratima, Kakdwip, Basanti, Sandeshkhali I and II, Hingalganj, Khejuri II, Moyna, Nandakumar, and Mahishadal (Fig. 10). These areas have comparatively high levels of WPR; and MA, pucca road among household members are gradually increased by the government because these blocks are facing frequent effect of TCs. Eleven CD Blocks in EM and two CD Blocks in Sundarbans have moderate adaptive capacity with an index value of −0.06 to 0.06 due to low literacy and low to moderate WPR and other indicators. However, initiatives by the Government of WB, such as 'emergency of cyclone shelter' and the increasing approach route by pucca road in the coastal blocks after the Aila cyclone in 2009, have helped to improve the adaptive capacity of the coastal blocks.

Cyclonic Vulnerability Index (CVI) along the West Bengal coast

The maximum value of CVI is 1.42, and the minimum is −0.65. The CVI values are classified into five classes based on Jenk natural breaks. Fig. 11 shows that twelve CD blocks have a potential vulnerability ranging from −0.65 to −0.36 due to their lower proximity to the drainage, lower forest cover, lower BUA, and low to moderate AC. The moderate vulnerable areas are included with the value −0.03 to 0.25 because of their moderate ELV, CL, BUA, and moderate LR. The highly vulnerable areas, with values ranging from 0.26 to 0.63, are those that have moderate to higher proximity to the drainage, moderate ELV, high PR, higher to moderate cultivated land, and insufficient AC to cope with cyclonic hazardous conditions. Three CD blocks are included in the very highly vulnerable area with a range of 0.64 to 1.42. Gosaba, Basanti, and Patharpratima CD blocks have a high EI and SI compared to their AC. The CVI map (Fig. 11) shows that EM is less vulnerable than ISR due to its AC. However, the effect of the cyclone was more pronounced in EM than in the Sundarbans.

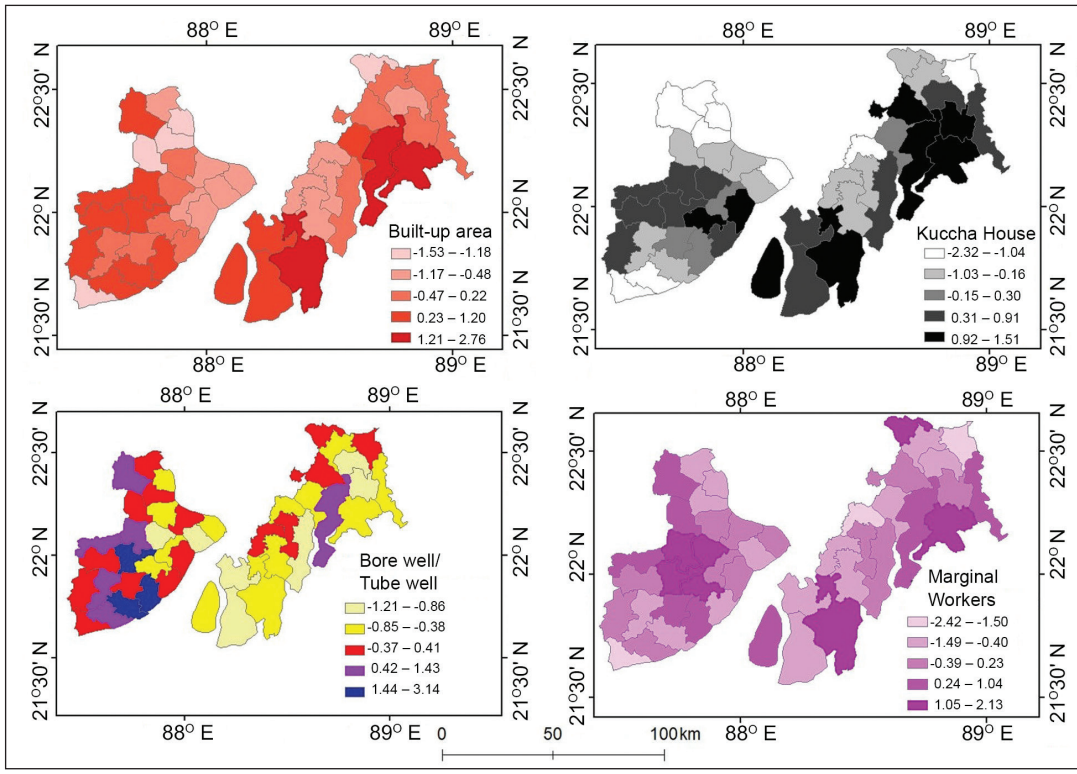

Figure 7. Spatial distribution of Sensitivity Index indicators mapped using standardised values to depict relative vulnerabilities across the study area.

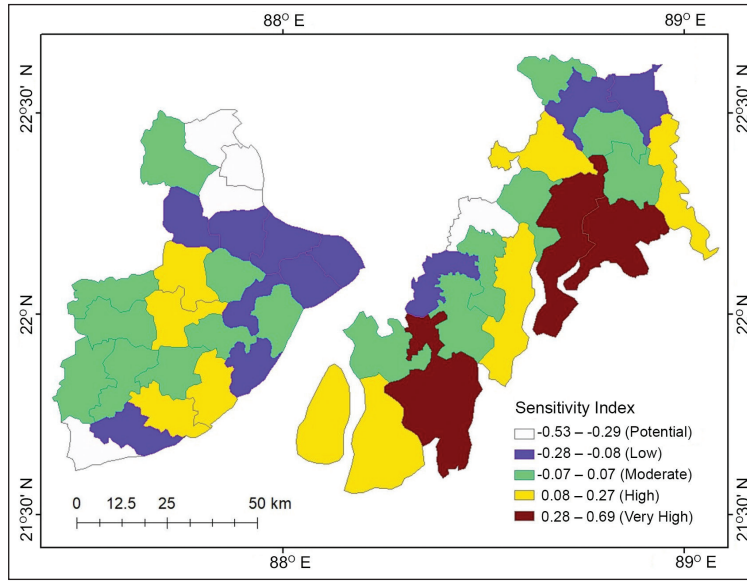

Figure 8. Spatial distribution of Sensitivity Index (SI) at the block level within the study area, highlighting differential vulnerability patterns based on standardised assessments.

Table 7. Pearson's Correlation Coefficient among the selected indicators..

	Correlations																							
Indicators	1	2	3	4	5	6	7	8	9	10	11	12	13	14	15	16	17	18	19	20	21	22	23	24
1. AFI	1.00																							
2. WS	−0.10	1.00																						
3. SS	0.06	0.45**	1.00																					
4. FD	0.25	−0.35*	0.20	1.00																				
5. FA	−0.16	0.18	0.07	0.22	1.00																			
6. PD	0.09	0.21	0.44**	0.45**	0.50**	1.00																		
7. ELV	−0.25	0.06	−0.33*	−0.71**	−0.15	−0.39**	1.00																	
8. IWB	0.36*	−0.41**	0.06	0.59**	0.19	0.34*	−0.52**	1.00																
9. DC	0.21	−0.64**	−0.17	0.86**	0.10	0.16	−0.54**	0.61**	1.00															
10. BUA	−0.06	0.36*	0.10	0.10	0.43**	0.53**	−0.13	−0.06	−0.05	1.00														
11. CL	−0.04	0.38*	0.33*	0.21	0.22	0.81**	−0.11	0.04	−0.03	0.44**	1.00													
12. KH	0.23	0.35*	0.21	0.17	0.27	0.45**	−0.36*	0.10	−0.04	0.59**	0.32*	1.00												
13. PR	−0.07	0.17	0.45**	0.64**	0.41**	0.62**	−0.64**	0.38*	0.40**	0.25	0.51**	0.38*	1.00											
14. DR	−0.05	0.13	0.14	−0.05	−0.16	−0.29*	0.01	−0.24	−0.08	−0.12	−0.18	−0.18	−0.08	1.00										
15. BW/TW	−0.18	0.05	−0.32*	−0.27	0.04	−0.29	0.26	−0.19	−0.16	0.19	−0.19	−0.13	−.32*	0.01	1.00									
16. MW	0.04	0.04	−0.05	0.00	0.05	0.34*	−0.10	0.07	−0.10	0.41**	0.25	0.59**	0.05	−0.21	0.11	1.00								
17. NLP	−0.06	−0.014	0.10	0.39**	0.31*	0.48**	−0.22	0.26	0.29*	0.54**	0.33*	0.20	.31*	−0.25	0.12	0.18	1.00							
18. LR	−0.12	0.18	0.07	−0.47**	−0.31*	−0.29	0.07	−0.22	−0.49**	−0.21	−0.19	−0.10	−0.27	0.20	0.17	0.03	−0.25	1.00						
19. MA	0.13	−0.018	0.29	0.09	0.12	0.48**	−0.15	0.20	0.00	0.06	0.33*	0.27	0.24	−0.15	−0.49**	0.23	0.03	−0.10	1.00					
20. SHA	0.14	0.43**	0.65**	0.48**	0.31*	0.79**	−0.54**	0.33*	0.18	0.51**	0.73**	0.43**	0.71**	−0.12	−0.24	0.09	0.45**	−0.19	0.30	1.00				
21. WPR	−0.06	0.43**	0.55**	−0.23	−0.12	−0.01	0.11	−0.25	−0.53**	0.10	0.00	0.22	−0.06	0.21	0.09	0.18	−0.01	0.33*	−0.04	0.12	1.00			
22. APR	0.10	0.24	0.55**	0.42**	0.05	0.54**	−0.53**	0.33*	0.21	0.11	0.49**	0.31*	0.57**	−0.11	−0.35*	0.12	0.29*	−0.09	0.52**	0.69**	0.11	1.00		
23. VHPS	−0.18	−0.35*	−0.49**	−0.59**	−0.19	−0.44**	0.59**	−0.19	−0.33*	−.38*	−0.36*	−0.51**	−0.64**	−0.08	0.32*	−0.00	−0.29	0.29	−0.06	−0.69**	−0.12	−0.50**	1	
24. TCM	0.24	−0.07	0.28	0.32*	−0.09	0.39**	−0.41**	0.39**	0.31*	0.01	0.31*	0.20	0.37*	−0.16	−0.39**	0.14	0.06	−0.09	.55**	0.47**	−0.18	0.70**	−0.32*	1

* Correlation is significant at the 0.05 level (2−tailed).

** Correlation is significant at the 0.01 level (2−tailed).

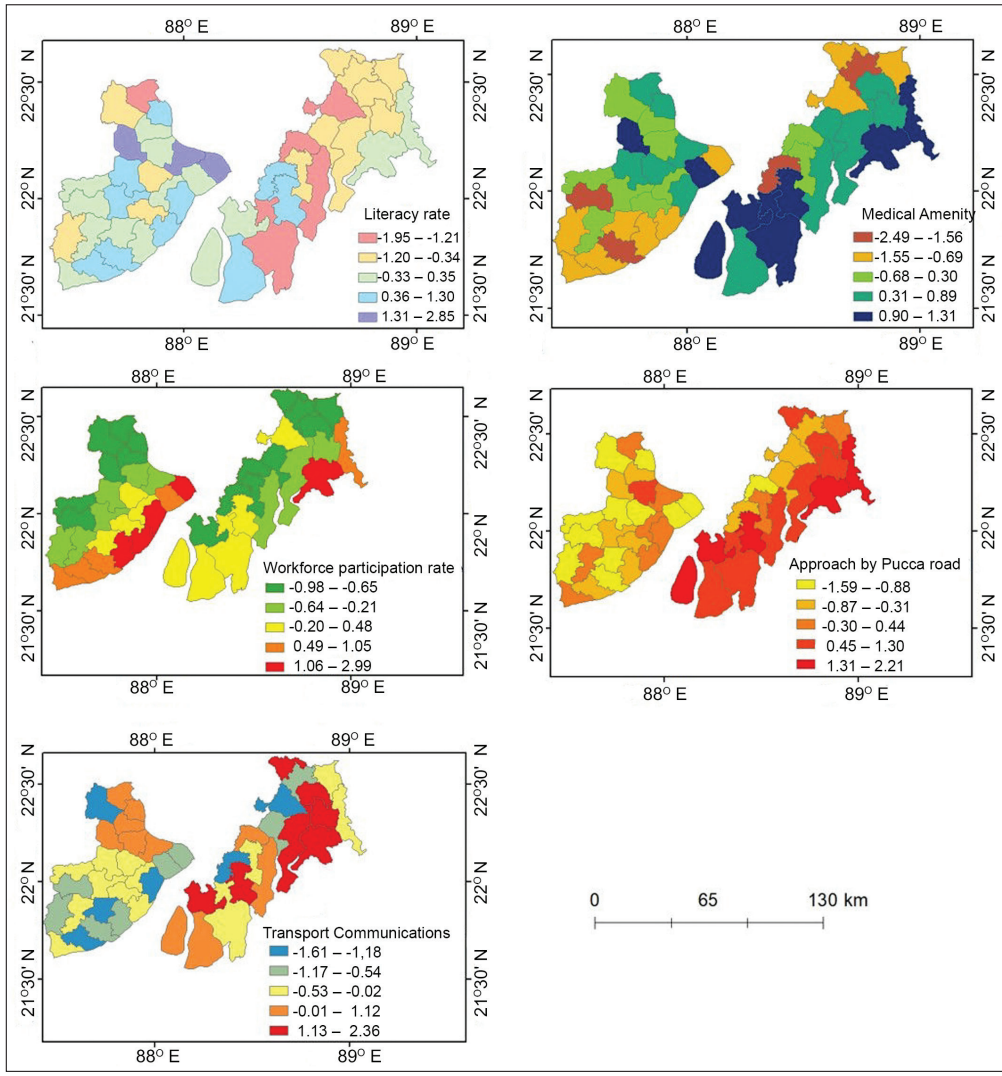

Figure 9. Spatial distribution of Adaptive Capacity Index (ACI) indicators mapped using standardised values to highlight resilience variations across the study area.

Discussion

Assessing socio-economic vulnerability for risk reduction necessitates a multidimensional and interdisciplinary approach (El-Zein and Tonmoy, 2015). This study employs a methodical framework to evaluate the direct and indirect impacts of severe cyclones on environmental assets, socio-economic conditions, and coastal communities. The composite vulnerability model, developed using Principal Component Analysis and weighting methods, provides a structured approach to cyclonic vulnerability assessment. By integrating indicators that reflect both natural and human influences, the model ensures a robust evaluation of vulnerability, with sampling adequacy tests enhancing the credibility of the results.

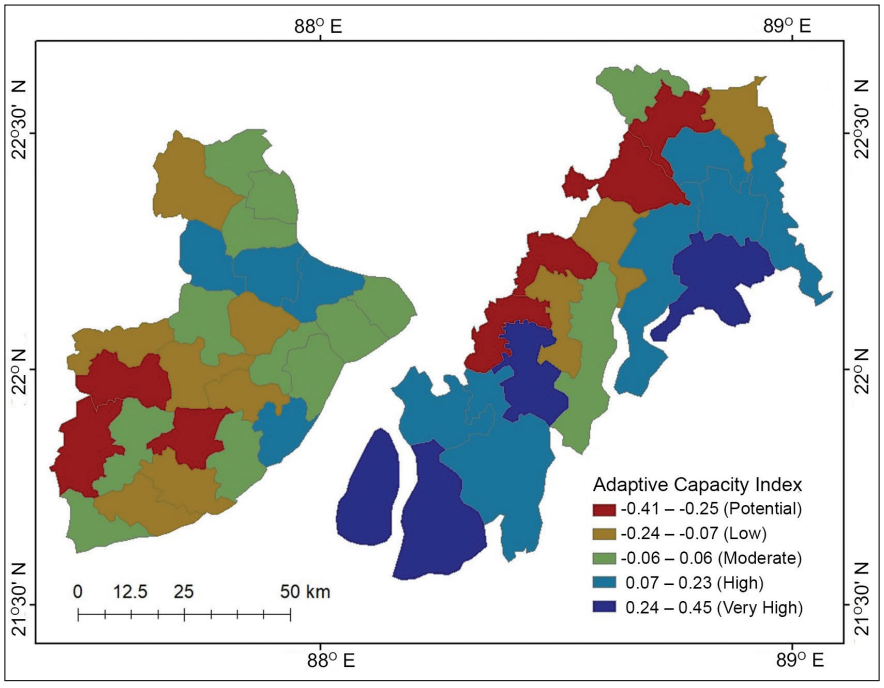

Figure 10. Spatial distribution of Adaptive Capacity Index (ACI) at the block level within the study area, highlighting resilience variations based on standardised assessments.

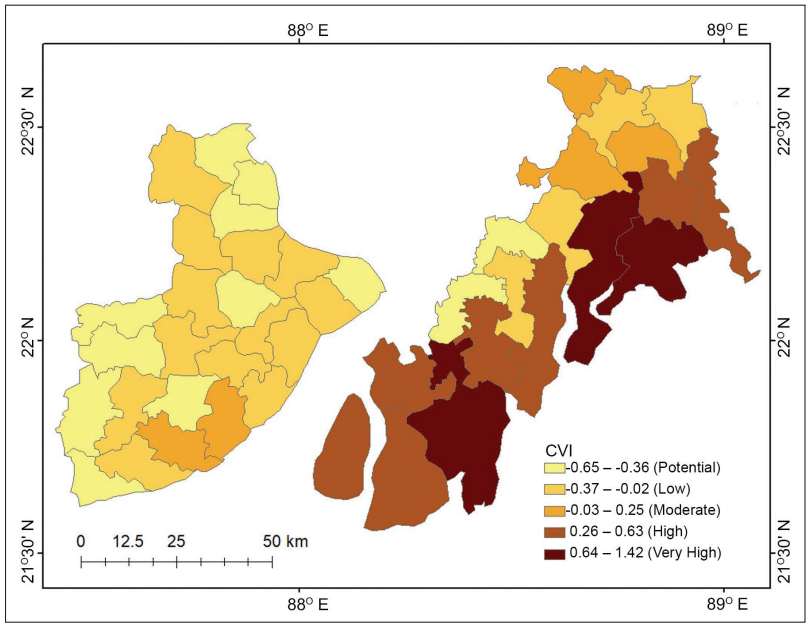

Figure 11. Spatial representation of Cyclonic Vulnerability Index (CVI) at the block level within the study area, highlighting differential exposure, sensitivity, and adaptive capacity based on standardised assessments.

At the block level, this model proves instrumental in environmental quality assessments, particularly in evaluating sustainable development, adaptive capacity, and resilience. The findings reveal significant variations in cyclonic vulnerability across different CD blocks, influenced by their connectivity to the mainland, proximity to the open coast, and exposure to physical hazards. Blocks with storm surge height, inundation levels, and lower elevation exhibit high to very high vulnerability due to increased exposure. Conversely, blocks characterised by dense built-up areas, extensive cultivated land, high poverty rates, marginal workers, and high dependency ratios demonstrate high sensitivity, further exacerbating their vulnerability. The adaptive capacity indicators ultimately determine the vulnerability status of each CD block, reinforcing the reliability of the composite model.

Globally, cyclonic vulnerability assessments have been conducted in various regions, each highlighting unique socio-environmental challenges. For instance, in the United States, studies emphasize the role of infrastructure resilience and early warning systems in mitigating cyclone impacts (Eberenz *et al.*, 2020). In the Philippines, vulnerability assessments underscore the importance of integrating storm surge modelling and rainfall-induced flooding into risk evaluations (Eberenz *et al.*, 2020). Similarly, research in Australia focuses on community-based adaptation strategies, leveraging local knowledge to enhance resilience (Ali *et al.*, 2020). These international perspectives reinforce the need for region-specific vulnerability models, as a single global framework may not adequately capture localised risk factors (Eberenz *et al.*, 2020).

Despite its strengths, this study acknowledges several limitations. Firstly, the PCA method effectively reduces dimensionality, and certain indicators may not fully capture the complexity of vulnerability dynamics. Secondly, cyclonic vulnerability is subject to change due to evolving climatic conditions, land use modifications, and socio-economic shifts. Thirdly, the composite vulnerability model is tailored to the study area and may require adjustments for application in other regions.

The findings of this study hold critical implications for policymakers (Nader *et al.*, 2008) and disaster management authorities (Patt *et al.*, 2005). By providing a quantifiable framework for vulnerability assessment, the model aids in targeted intervention strategies, ensuring that resources are allocated efficiently to high-risk areas. The insights gained from this research can inform climate adaptation policies, emphasising sustainable land use planning, infrastructure resilience, and socio-economic empowerment. Furthermore, integrating international best practices into local vulnerability assessments can enhance disaster preparedness and mitigation strategies, fostering a more resilient coastal environment.

This study underscores the urgent need for proactive measures to address climate change-induced cyclonic events. As cyclonic storms continue to intensify, their socio-economic repercussions will become more pronounced, necessitating comprehensive risk assessments and adaptive strategies. By refining vulnerability models and incorporating global perspectives, future research can contribute to more effective disaster management frameworks, ensuring long-term resilience for vulnerable coastal communities.

Conclusion

Climatic events can create hazardous situations, and it is important to raise awareness through observation and media attention. This assessment can help in planning for future mitigation strategies at the local level. This paper presents the results of a cyclonic vulnerability assessment for the tropical cyclones between 2001 to 2024 along the WB coast. This assessment was based on exposure, sensitivity, and AC indicators recommended by the IPCC framework for vulnerability assessment. We used composite indicators that were easily obtained from secondary sources. Statistical analysis showed that exposure and AC indicators are crucial in determining the CVI. Although the track and intensity of cyclones may vary, this study provides a comprehensive understanding of the hazardous and vulnerable situation of the study area, which can be a valuable reference for planners. Therefore, future studies should continue to improve the indicator system and collect new data for coastal management. In conclusion, while considering cyclonic events, the study area can reduce vulnerability by improving AC such as LR, PR, MA, TCM facilities. By raising awareness among the local people, the government can help to increase efficiency for better management of such situations.

Acknowledgment

The authors would like to thank the Local Government body and the census authority for providing data and other necessary secondary data collection. They are also grateful to the USGS for making Landsat and Sentinel data publicly accessible. Thanks to Chitralekha Das for helping them create maps from Sentinel 1 images. Other thanks to the local people of the study area and the Department of Geography of West Bengal State University. Lastly, the authors appreciate the editor and reviewers for their insightful recommendations, which have significantly enhanced the quality of the manuscript.

References

Ali, S.A., Khatun, R., Ahmad, A. and Ahmad, S.N. (2020) Assessment of cyclone vulnerability, hazard evaluation and mitigation capacity for analyzing cyclone risk using GIS technique: A study on Sundarban biosphere reserve, India. *Earth Systems and Environment*, 4: 71−92. https://doi.org/10.1007/s41748-019-00140-x.

Bandyopadhyay, S. (2007) Evolution of the Ganga Brahmaputra delta: a review. *Geographical review of India*, 69(3): 235−268.

Behera, M.D., Prakash, J., Paramanik, S., Mudi, S., Dash, J., Varghese, R. and Srivastava, P. K. (2022) Assessment of tropical cyclone Amphan-affected inundation areas using sentinel-1 satellite data. *Tropical Ecology*, 63(1): 9−19. https://doi.org/10.1007/s42965-021-00187-w.

Below, T.B., Mutabazi, K.D., Kirschke, D., Franke, C., Sieber, S., Siebert, R. and Tscherning, K. (2012) Can farmers' adaptation to climate change be explained by socio-economic household-level variables? *Global environmental change*, 22(1): 223−235. https://doi.org/10.1016/j.gloenvcha.2011.11.012.

Bhakat, R.K. (2001) Coastal Dune of Digha, India—A Plea for Continued Protection. *Indian Journal of Geography and Environment*, 6: 54−60.

Bjarnadottir, S., Li, Y. and Stewart, M. G. (2011) Social vulnerability index for coastal communities at risk to hurricane hazard and a changing climate. *Natural Hazards*, 59: 1055−1075. https://doi.org/10.1007/s11069-011-9817-5.

Census of India (2011) *Primary census abstract, census of India*. The government of India, Registrar General and Census Commissioner

of India, Ministry of Home Affairs, New Delhi, India.

Chen, J., Wang, Z., Tam, C.Y., Lau, N.C., Lau, D.S.D. and Mok, H.Y. (2020) Impacts of climate change on tropical cyclones and induced storm surges in the Pearl River Delta region using pseudo-global-warming method. *Scientific Reports*, 10(1): 1−10. https://doi.org/10.1038/s41598-020-58824-8.

Chittibabu, P., Dube, S.K., Macnabb, J.B., Murty, T.S., Rao, A.D., Mohanty, U.C. and Sinha, P.C. (2004) Mitigation of flooding and cyclone hazard in Orissa, India. *Natural Hazards*, 31(2): 455−485. https://doi.org/10.1023/B:NHAZ.0000023362.26409.22.

Cutter, S.L., Boruff, B.J. and Shirley, W.L. (2003) Social vulnerability to environmental hazards. *Social science quarterly*, 84(2): 242−261. https://doi.org/10.1111/1540-6237.8402002.

Das, S, Das, A, Kar, N.S. and Bandyopadhyay, S. (2020) Cyclone Amphan and its impact on the Lower Deltaic West Bengal: a preliminary assessment using remote sensing sources. *Current Science*, 119(8): 1246–1249.

Das, R., and Dandapath, P. (2014) Existence and experience of Purba Medinipur coastal belt on its morpho−dynamic journey with the distinctive geology and geomorphology. *International Journal of Science and Research*, 3(6): 1242−1251.

De Dominicis, M., Wolf, J., Jevrejeva, S., Zheng, P. and Hu, Z. (2020) Future interactions between sea level rise, tides, and storm surges in the world's largest urban area. *Geophysical Research Letters*, 47(4): 1–11. e2020GL087002. https://doi.org/10.1029/2020GL087002.

Duan, W., Yuan, J., Duan, X. and Feng, D. (2021) Seasonal variation of tropical cyclone genesis and the related large-scale environments: Comparison between the Bay of Bengal and Arabian Sea sub-basins. *Atmosphere*, 12(12): 1−20. https://doi.org/10.3390/atmos12121593.

Eberenz, S., Lüthi, S., and Bresch, D.N. (2020) Regional tropical cyclone impact functions for globally consistent risk assessments. *Natural Hazards and Earth System Sciences Discussions*, 2020: 393–415. https://doi.org/10.5194/nhess−21−393−2021.

EEA (2006) *The changing faces of Europe's coastal areas*. E. Report (Ed.): 107p.

El-Zein, A. and Tonmoy, F.N. (2015) Assessment of vulnerability to climate change using a multicriteria outranking approach with application to heat stress in Sydney. *Ecological Indicators*, 48: 207−217.

Gupta, K. (2020) Challenges in developing urban flood resilience in India. *Philosophical Transactions of the Royal Society A*, 378(2168), 20190211. https://doi.org/10.1098/rsta.2019.0211.

Haldar, P., Karmakar, S. and Roy, S. (2021) Effect of Super Cyclone Amphan on Structure: A Case Study. In Timbadiya, P.V., M. C. Deo, M.C. and Singh, V.P. (ed) *Coastal, Harbour and Ocean Engineering, Proceedings of the International Conference on Hydraulics, Water Resources and Coastal Engineering*: 229−241.

Hassan, M.M., Ash, K., Abedin, J., Paul, B. K. and Southworth, J. (2020) A quantitative framework for analyzing spatial dynamics of flood events: a case study of super cyclone Amphan. *Remote Sensing*, 12(20): 3454. https://doi.org/10.3390/rs12203454.

Hinkel, J. (2011) "Indicators of vulnerability and adaptive capacity": towards a clarification of the science-policy interface. *Global environmental change*, 21(1): 198−208.

Hoque, M.A.A., Phinn, S., Roelfsema, C. and Childs, I. (2016) Assessing tropical cyclone impacts using object-based moderate spatial resolution image analysis: a case study in Bangladesh. *International Journal of Remote Sensing*, 37(22): 5320−5343.

Hoque, M.A.A., Pradhan, B., Ahmed, N., Ahmed, B. and Alamri, A.M. (2021) Cyclone vulnerability assessment of the western coast of Bangladesh. *Geomatics, Natural Hazards and Risk*, 12(1): 198−221.

Hufschmidt, G. (2008) *The evolution of risk from landslides: concepts and applications for communities in New Zealand*. Victoria University of Wellington: 503p.

IPCC (2007) *Climate Change 2007: The Physical Science Basis*. Summary for Policymakers Contribution of Working Group I to the Fourth Assessment Report of the Intergovernmental Panel on Climate Change, Geneva: 18p.

Joy, J., Kanga, S., and Singh, S.K. (2019) Kerala flood 2018: flood mapping by participatory GIS approach, Meloor Panchayat. *International Journal on Emerging Technologies*, 10(1): 197−205.

Kaiser, H.F. and Rice, J. (1974) Little jiffy, mark IV. *Educational and psychological measurement*, 34(1): 111−117. https://doi.org/10.1177/001316447403400115.

Kanga, S. and Singh, S.K. (2017) Mapping of salt affected and waterlogged areas using geospatial technique. *International Journal on Recent and Innovation Trends in Computing and Communication*, 5: 1298−1305.

Kanga, S., Meraj, G., Das, B., Farooq, M., Chaudhuri, S. and Singh, S.K. (2020) Modelling the spatial pattern of sediment flow in lower Hugli estuary, West Bengal, India by quantifying suspended sediment concentration (SSC) and depth conditions using geoinformatics. *Applied Computing and Geosciences,* 8, 100043: 1–12. https://doi.org/10.1016/j.acags.2020.100043.

Kar, N.S. and Bandyopadhyay, S. (2015) Tropical storm Aila in Gosaba block of Indian Sundarban: remote sensing based assessment of impact and recovery. *Geographical Review of India*, 77(1): 40−54.

Kleinosky, L.R., Yarnal, B. and Fisher, A. (2007) Vulnerability of Hampton Roads, Virginia to storm-surge flooding and sea-level rise. *Natural hazards*, 40: 43−70.

Kotzee, I. and Reyers, B. (2016) Piloting a social-ecological index for measuring flood resilience: A composite index approach. *Ecological indicators*, 60: 45−53.

Krishnamurthy, P.K., Choularton, R.J., Betts, R. and Lewis, K. (2011) *Assessing the impacts of climate risk on food security through a vulnerability index*. In Vulnerability Workshop of GI Forum 2011, Salzburg, Austria.

Lavell, A., Oppenheimer, M., Diop, C., Hess, J., Lempert, R., Li, J. and Weber, E. (2012) Climate change: new dimensions in disaster risk, exposure, vulnerability, and resilience. In *Managing the risks of extreme events and disasters to advance climate change adaptation: Special report of the intergovernmental panel on climate change,* Cambridge University Press: 25−64.

McGranahan, G., Balk, D. and Anderson, B. (2007) The rising tide: assessing the risks of climate change and human settlements in low elevation coastal zones. *Environment and Urbanization,* 19(1): 17−37.

Mishra, M., Acharyya, T., Santos, C.A.G., Marques da Silva, R. Kar, D., Kamal, A. H. M. and Raulo, S. (2021) Geo-ecological impact assessment of severe cyclonic storm Amphan on Sundarban mangrove forest using geospatial technology. *Estuarine, Coastal and Shelf Science*, 260: 107486. https://doi.org/10.1016/j.ecss.2021.107486.

Mondal, M., Biswas, A., Haldar, S., Mandal, S., Bhattacharya, S. and Paul, S. (2022) Spatio-temporal behaviours of tropical cyclones over the Bay of Bengal Basin in last five decades. *Tropical Cyclone Research and Review*, 11(1): 1−15.

Mondal, M., Haldar, S., Biswas, A., Mandal, S., Bhattacharya, S., and Paul, S. (2021) Modelling cyclone-induced multi-hazard risk assessment using analytical hierarchical processing and GIS for coastal West Bengal, India. *Regional Studies in Marine Science*, 44: 101779.

Nader, M.R., Abi Salloum, B. and Karam, N. (2008) Environment and sustainable development indicators in Lebanon: a practical municipal level approach. *Ecological indicators*, 8(5): 771−777.

Patt, A., Klein, R.J. and de la Vega-Leinert, A. (2005) Taking the uncertainty in climate-change vulnerability assessment seriously. *Comptes Rendus Geoscience*, 337(4): 411−424.

Patwardhan, A., Semenov, S., Schnieder, S., Burton, I., Magadza, C., Oppenheimer, M. and Sukumar, R. (2007) Assessing key vulnerabilities and the risk from climate change. *Climate change*: 779−810.

Paul, S., and Chowdhury, S. (2021). Investigation of the character and impact of tropical cyclone Yaas: a study over coastal districts of West Bengal, *India. Safety in Extreme Environments*, 3(3): 219−235.

Riitters, K.H., O'neill, R.V., Hunsaker, C.T., Wickham, J.D., Yankee, D.H., Timmins, S.P. and Jackson, B.L. (1995) A factor analysis of landscape pattern and structure metrics. *Landscape Ecology*, 10: 23−39.

Romieu, E., Welle, T., Schneiderbauer, S., Pelling, M. and Vinchon, C. (2010) Vulnerability assessment within climate change and natural hazard contexts: revealing gaps and synergies through coastal applications. *Sustainability Science*, 5: 159−170.

Rubinato, M., Heyworth, J. and Hart, J. (2020) Protecting coastlines from flooding in a changing climate: A preliminary experimental study to investigate a sustainable approach. *Water,* 12(9): 2471.

Sharma, S.S.P., Rao, K.D., and Shukla, A.K. (2020) Near real-time delineation, mapping and monitoring of floods in West Bengal, India due to extremely severe cyclone 'Amphan' using multi-mission satellite data. *Current Science*, 119(12): 1939.

Shoji, M. and Murata, A. (2021) Social capital encourages disaster evacuation: evidence from a cyclone in Bangladesh. *The Journal of Development Studies*, 57(5): 790−806.

Siegel, F.R. (2020) An example of coastal cities hazard exposure and economics. In *Adaptations of coastal cities to global warming, sea level rise, climate change and endemic hazards*, Springer Briefs in Environmental Science, Springer, Cham: 63−69. https://doi.org/10.1007/978-3-030-22669-5_7.

Smit, B. and Wandel, J. (2006) Adaptation, adaptive capacity and vulnerability. *Global Environmental Change*, 16(3): 282−292.

Ummenhofer, C.C. and Meehl, G.A. (2017) Extreme weather and climate events with ecological relevance: a review. *Philosophical Transactions of the Royal Society B: Biological Sciences*, 372(1723): 20160135. https://doi.org/10.1098/rstb.2016.0135.

Wong, K.Y., Yip, C.L. and Li, P.W. (2008) Automatic tropical cyclone eye fix using genetic algorithm. *Expert Systems with Applications*, 34(1): 643−656.

Wu, T. (2021) Quantifying coastal flood vulnerability for climate adaptation policy using principal component analysis. *Ecological Indicators*, 129, 108006. https://doi.org/10.1016/j.ecolind.2021.108006.

Xia, M., Jia, K., Zhao, W., Liu, S., Wei, X. and Wang, B. (2021) Spatio-temporal changes of ecological vulnerability across the Qinghai-Tibetan Plateau. *Ecological Indicators*, 123, 107274. https://doi.org/10.1016/j.ecolind.2020.107274.

Date received: 10 March 2025
Date accepted after revision: 27 October 2025